Evolution of organogenesis. Our findings suggest that a complex gene network regulated by PHA-4 could have evolved by serial recruitment of target genes. If the digestive tract of primitive organisms was a simple epithelial sac, then direct targets of ancestral PHA-4 may have been those that encoded digestive enzymes and those required to form epithelia. As additional genes, including transcription factors, fell under PHA-4 control, patterns of gene expression within the resulting organ structures may have increased in complexity. This model provides a possible explanation for the fact that FoxA proteins play a conserved role in foregut development in animals whose foreguts are morphologically and mechanistically different from one another. FoxA proteins may have acquired different target genes in different organisms, enabling new cell types or morphologies to emerge.

References and Notes

1. R. Schnabel, J. Priess, in *C. elegans II*, D. L. Riddle, T. Blumenthal, B. J. Meyer, J. R. Priess, Eds. (Cold Spring Harbor Press, Cold Spring Harbor, NY, 1997), pp. 361–382.
2. M. Labouesse, S. E. Mango, *Trends Genet*. **15**, 307 (1999).
3. M. F. Portereiko, S. E. Mango, *Dev. Biol*. **233**, 482 (2001).
4. D. G. Albertson, J. N. Thomson, *Philos. Trans. R. Soc. London Ser. B* **275**, 299 (1976).
5. J. E. Sulston *et al*., *Dev. Biol*. **100**, 64 (1983).
6. M. A. Horner *et al*., *Genes Dev*. **12**, 1947 (1998).
7. S. E. Mango, E. J. Lambie, J. Kimble, *Development* **120**, 3019 (1994).
8. J. M. Kalb *et al*., *Development* **125**, 2171 (1998).
9. E. Kaufmann, W. Knochel, *Mech. Dev*. **57**, 3 (1996).
10. V. Reinke *et al*., *Mol. Cell* **6**, 605 (2000).
11. K. J. Kemphues, K. J. Priess, D. G. Morton, N. Cheng, *Cell* **52**, 311 (1988).
12. B. Bowerman, B. A. Eaton, J. R. Priess, *Cell* **68**, 1061 (1992).
13. Detailed protocols and a list of genes with a *par-1/skn-1* ratio ≥2 are available on *Science* Online at www.sciencemag.org/cgi/content/full/295/5556/821/DC1.
14. P. G. Okkema, A. Fire, *Development* **120**, 2175 (1994).
15. In situ hybridization data are available at Y. Kohara's Nematode Expression Pattern DataBase (http://nematode.lab.nig.ac.jp/).
16. D. G. Overdier, A. Porcella, R. H. Costa, *Mol. Cell. Biol*. **14**, 2755 (1994).
17. J. A. Dent, M. W. Davis, L. Avery, *EMBO J*. **16**, 5867 (1997).
18. Y. Shibata, T. Fujii, J. A. Dent, H. Fujisawa, S. Takagi, *Genetics* **154**, 635 (2000).
19. J. D. Thatcher, A. P. Fernandez, L. Beaster-Jones, C. Haun, P. G. Okkema, *Dev. Biol*. **229**, 480 (2001).
20. J. Gaudet, S. E. Mango, data not shown.
21. L. Avery, *Genetics* **133**, 897 (1993).
22. We define six developmental stages as follows: "v. early" = before the formation of the pharynx primordium; "early" = formation of the pharynx primordium; "mid" = during pharynx elongation; "mid-late" = after attachment of the pharynx to the buccal cavity but before the separation of the two lobes of the pharynx; "late" = the two lobes of the pharynx are distinguishable, but the pharynx is not fully formed; and "v. late" = the pharynx is fully developed though not yet functional.
23. J. Rusch, M. Levine, *Curr. Opin. Genet. Dev*. **6**, 416 (1996).
24. Y. T. Ip, M. Levine, S. J. Small, *J. Cell Sci. Suppl*. **16**, 33 (1992).
25. K. Zaret, *Dev. Biol*. **209**, 1 (1999).
26. G. Jurgens, D. Weigel, *Roux's Arch. Dev. Biol*. **197**, 345 (1988).
27. M. Lehmann, G. Korge, *EMBO J*. **15**, 4825 (1996).
28. S. L. Ang, J. Rossant, *Cell* **78**, 561 (1994).
29. D. C. Weinstein *et al*., *Cell* **78**, 575 (1994).
30. K. A. Guss, C. E. Nelson, A. Hudson, M. E. Kraus, S. B. Carroll, *Science* **292**, 1164 (2001).
31. W. J. Gehring, K. Ikeo, *Trends Genet*. **15**, 371 (1999).
32. D. M. Miller, F. E. Stockdale, J. Karn, *Proc. Natl. Acad. Sci. U.S.A*. **83**, 2305 (1986).
33. J. P. Ardizzi, H. F. Epstein, *J. Cell Biol*. **105**, 2763 (1987).
34. J. Y. Sze, M. Victor, C. Loer, Y. Shi, G. Ruvkun, *Nature* **403**, 560 (2000).
35. Y. Cheng, W. H. Prusoff, *Biochem. Pharmacol*. **22**, 3099 (1973).

36. We are indebted to S. Kim, R. Begley, C. van Doren, K. Duke, and M. Jiang, who generated microarrays and performed hybridization experiments, and to M. Horner, who made the first RNA samples. We also thank B. Bowerman, A. Fire, K. Kemphues, G. Seydoux, and E. Jorgensen for strains and plasmids; B. Graves for advice on EMSA; A. Tsodikov for advice on statistics; and B. Graves, M. Lehmann, C. Thummel, J. Saam, and S. Lange for comments on the manuscript. Funding was provided by a Canadian Institutes of Health Research postdoctoral fellowship (J.G.) and by NIH grants R01 GM056264 and CCSG 2P30CA42014 (S.E.M.). S.E.M. is an assistant investigator of the Huntsman Cancer Institute Center for Children.

7 August 2001; accepted 13 December 2001

Tunneling Spectroscopy of the Elementary Excitations in a One-Dimensional Wire

O. M. Auslaender,[1]* A. Yacoby,[1] R. de Picciotto,[2] K. W. Baldwin,[2] L. N. Pfeiffer,[2] K. W. West[2]

The collective excitation spectrum of interacting electrons in one dimension has been measured by controlling the energy and momentum of electrons tunneling between two closely spaced, parallel quantum wires in a GaAs/AlGaAs heterostructure while measuring the resulting conductance. The excitation spectrum deviates from the noninteracting spectrum, attesting to the importance of Coulomb interactions. An observed 30% enhancement of the excitation velocity relative to noninteracting electrons with the same density, a parameter determined experimentally, is consistent with theories on interacting electrons in one dimension. In short wires, 6 and 2 micrometers long, finite size effects, resulting from the breaking of translational invariance, are observed.

Electronic systems such as metals contain a vast number of mobile electrons. Surprisingly, despite the Coulomb repulsion between them, many electronic properties of metals can be well described in terms of independent particles with a finite lifetime, each carrying charge e and spin half (*1*, *2*). Most importantly, their excitation spectrum, which for noninteracting electrons is simply determined by the underlying band mass m, is only slightly modified by the Coulomb interactions.

However, such a simple description of electronic systems, known as Landau Fermi-liquid theory (*1*), is valid only in two and three spatial dimensions. In one-dimensional (1D) metals, where electrons are forced to move on a line, the single-particle description completely breaks down by even the slightest Coulomb repulsion. Instead, the excitations of an interacting 1D system, being fluctuations of the charge and spin densities, are well described by collective modes that involve the entire electron population (*3*). These collective modes are decoupled into two separate kinds: collective spin modes and collective charge modes. Coulomb interactions couple primarily to the latter, thereby strongly influencing their dispersion. Conversely, the excitation spectrum of the spin modes, typically unaffected by interactions, remains similar to the noninteracting case. For example, low-energy charge excitations propagate with velocity $v_p = v_F/g$, where $v_F = \hbar k_F/m$ is the Fermi velocity ($\hbar = h/2\pi - h$ is Planck's constant, and k_F is the Fermi wave vector). The parameter g, which characterizes the interactions, is given by $g \approx \{1+[U/(2E_F)]\}^{-1/2}$, where U is the Coulomb interaction energy between particles in the wire and E_F is the Fermi energy (*4*). Thus, the stronger the Coulomb repulsion is, the larger the propagation velocity is.

Although interactions fundamentally alter the excitation spectrum of a 1D wire, they do not affect its conductance (*5*–*10*). In fact, a clean 1D wire has universal conductance irrespective of its length, density, and dispersion (*11*), ren-

[1]Department of Condensed Matter Physics, Weizmann Institute of Science, Rehovot 76100, Israel. [2]Bell Labs, Lucent Technologies, 700 Mountain Avenue, Murray Hill, NJ 07974, USA.

*To whom correspondence should be addressed. E-mail: ophir.auslaender@weizmann.ac.il

dering transport measurements an ineffective tool for investigating the role of interactions in one dimension. This limitation can be circumvented by studying the temperature-dependent transport properties of disordered wires (*12*–*15*). However, the lack of knowledge of the nature of the disorder potential often restricts the interpretation of such experiments. Therefore, the most direct way to explore the role of interactions in one dimension is to measure the excitation spectrum itself.

We report a method for experimentally determining the complete dispersion relations of the collective elementary excitations of an interacting 1D system, in which the tunneling conductance between two clean, parallel wires is measured. A fixed amount of energy and momentum is supplied to the system by externally applying a bias between the wires (V_{sd}) and a magnetic field (B) perpendicular to their plane. Because of the conservation of energy and momentum in our geometry, tunneling is forbidden unless there exist elementary excitations that match the supplied momentum and energy.

The spectrum of elementary excitations has been previously studied with Raman spectroscopy (*16*, *17*). However, that technique is limited to excitations with very low momenta, whereas our method allows us to determine the spectrum of elementary excitations to energies that far exceed E_F and momenta much larger than $2k_F$. Our measurements show that throughout the entire measured phase space, the dispersion relations of the elementary excitations deviate substantially from the noninteracting predictions, attesting to the collective nature of the excitations.

The two parallel 1D wires are fabricated by cleaved edge over growth (CEO) from a GaAs/AlGaAs double quantum well (QW) heterostructure (*18*). The upper QW is 20 nm wide, the lower one is 30 nm wide, and they are separated by a 6-nm AlGaAs barrier ≈300 meV high. A modulation doping sequence is used, which renders only the upper QW occupied by a two-dimensional electron gas (2DEG) with a density $n \approx 2 \times 10^{11}$ cm^{-2} and a mobility $\mu > 3 \times 10^6$ cm^2 V^{-1} s^{-1}. The CEO creates two quantum wires in the two QWs along the whole edge of the sample. Both wires are tightly confined on three sides by atomically smooth planes and on the fourth side by a triangular potential formed at the cleaved edge. The 2DEG overlaps the upper quantum wire (UQWR) and is separated from the lower quantum wire (LQWR) by the tunnel barrier separating the two QWs.

The measurement of a single, isolated tunnel junction between the wires is facilitated by controlling the density of electrons under tungsten top gates. The 2-μm-wide gates are deposited before the cleave at a distance of 2 μm from each other (Fig. 1). First, we bias gate g_2 while monitoring the two-terminal conductance (G) between contacts to the 2DEG on opposite sides of it (*19*). When the voltage on g_2 relative to the 2DEG (V_2) is negative enough to deplete the 2DEG, G drops sharply because the electrons have to scatter into the wires to pass under g_2. As tunneling into the LQWR is weak, most of the current is carried at this stage by the UQWR. Decreasing V_2 further depletes the modes in the UQWR under g_2 one by one, causing a stepwise decrease in G (Fig. 2). The deviation of the size of the steps from the universal $G_0 = 2e^2/h$, in which e is the charge of the electron, is known to be related to the nature of the coupling between the 2DEG and the UQWR (*6*, *20*, *21*); however, a complete explanation is still lacking. When the last mode in the UQWR is depleted, only LQWR modes are left to carry current, leaving a very small conductance step (typically a few percent of the UQWR conductance steps).

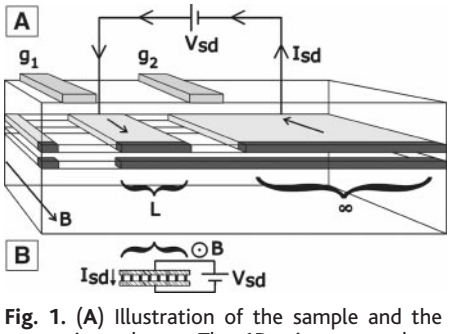

Fig. 1. (**A**) Illustration of the sample and the contacting scheme. The 1D wires span along the whole cleaved edge of the sample (front side in the schematic). A barrier separates the lower wire from the upper wire (dark gray) and the 2DEG that overlaps it (light gray). The 2DEG is used to contact both wires. Several tungsten top gates can be biased to deplete the electrons under them (only g_1 and g_2 are shown). A magnetic field B is perpendicular to the wires' plane. The depicted configuration allows the study of the conductance of a single wire-wire tunnel junction of length L. (**B**) Equivalent circuit of the measurement configuration: The current flows uniformly between the wires along the whole length of the junction.

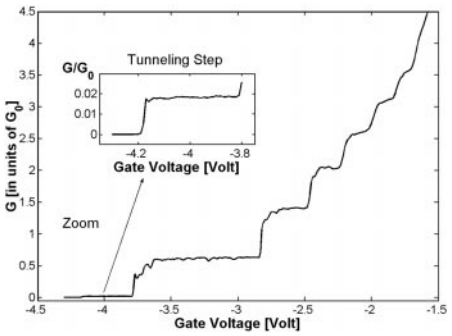

Fig. 2. Conductance as a function of the density in the wires at $B = 0$, controlled through the voltage on a top gate. The UQWR conductance steps can be seen clearly. (**Inset**) The residual conductance (less than 1/30 of the previous conductance step) after the UQWR has been depleted is attributed to transport that involves tunneling into the LQWR.

Decreasing V_2 further depletes these modes as well, and G is suppressed to zero. We then choose a value of V_2 on the tunneling step, forcing the electrons to tunnel between the wires. To focus on one of the two resultant junctions, we reduced the length of one of them by depleting both wires with an additional gate (g_1 in Fig. 1). Because the short tunnel junction is much more resistive than the long one, the UQWR between g_1 and g_2 is at electrochemical equilibrium with the source (the 2DEG lying between g_1 and g_2), and the LQWR is at electrochemical equilibrium with the drain (the semi-infinite 2DEG to the right of g_2 in Fig. 1). As a result, V_{sd} drops across an isolated wire-wire tunnel junction of length L (the distance between g_1 and g_2).

Measuring the tunneling current through a single tunnel junction allows us to experimentally determine the dispersion relations of the elementary excitations in the wires (*22*, *23*). The junction is long enough for tunneling to be spatially invariant to a good approximation ($L \gg \lambda_F$, where λ_F is a typical Fermi wavelength in the wires). Therefore, when an electron tunnels between the wires, not only its energy is conserved, but also its momentum $\hbar k$, where k is the wave vector. The energy of a tunneling electron is controlled by changing V_{sd}, whereas its momentum is controlled by changing B (*24*). This is true regardless of electron-electron interactions, be they intrawire or interwire. To first order, B shifts the dispersions of the modes in the UQWR, $E_{u_i}(B,k)$, by $k_B = eBd/\hbar$ (u_i enumerates the modes of the UQWR and d is the distance between the wires' centers) relative to the dispersions of the modes in the LQWR, $E_{l_j}(B,k)$ (l_j enumerates the modes of the LQWR). Tunneling between the wires is suppressed unless there is a k that satisfies the tunneling condition: $E_{u_i}(B,k - k_B) = E_{l_j}(B,k) - eV_{sd}$, for which one wire is occupied while the other is not. Thus, current is appreciable only in regions of the V_{sd}-B plane that are bounded by $B(V_{sd})$ that satisfies the tunneling condition with $|k|$ or $|k - k_B|$ equal to one of the Fermi wave numbers of one of the modes in the wires, k_{F,u_i} or k_{F,l_j}. These boundaries show up as peaks in the nonlinear differential tunneling conductance $G(V_{sd},B)$; i.e., the measurement directly probes the dispersion of one wire with the help of the Fermi points of the other wire (see Fig. 3B). It has been shown theoretically that even in the presence of interactions, this measurement technique is viable: It allows direct measurement of the collective excitation spectrum of the interacting system (*25*, *26*). In addition, the k difference that we can induce between the wires has no fundamental limitation—it is easy to attain $k_B > 2k_F$ with reasonable B's. In typical measurements (Fig. 3, A and C), the most prominent features are the dispersion curves of the elementary excitations in the wires.

To determine the effect of the Coulomb interactions on the excitation spectrum, we

compare $G(V_{sd},B)$ scans with the excitation spectrum of noninteracting electrons. The latter is solely determined by the band mass m and by the density of electrons. Consider, for example, tunneling of noninteracting electrons between mode u_i and mode l_j. At $B = 0$, tunneling is expected to be substantial only if the dispersion in u_i overlaps that in l_j; otherwise, it is impossible for an electron to tunnel while conserving its energy and momentum. To compensate for a density mismatch between the modes, a bias $V^*_{sd} = (E_{F,l_j} - E_{F,u_i})/e$ must be applied for the dispersions to overlap (E_{F,u_i} and E_{F,l_j} are the Fermi energies in u_i and l_j). Thus, a point of enhanced current is expected on the V_{sd} axis (see Fig. 3B). Several such points can be seen in Fig. 3, A and C, each corresponding to tunneling between a different pair of modes. Tunneling between the modes is also possible near $V_{sd} = 0$. For simplicity, consider wires with vanishing cross section, for which B does not influence the Fermi wave numbers of the modes. As B is ramped up, the spectra are shifted by k_B relative to one another. Initially, tunneling remains rare because the available initial states are unoccupied. This persists until $k^{i,j}_{B_1} \equiv edB^{i,j}_1/(h/2\pi) = |k_{F,u_i} - k_{F,l_j}|$, when initial states become available at the Fermi level, allowing tunneling between states propagating in the same direction. Increasing B further blocks the tunneling because now all available final states are occupied until B satisfies $k^{i,j}_{B_2} \equiv edB^{i,j}_2/(h/2\pi) = |k_{F,u_i} + k_{F,l_j}|$, when empty final states become available at the Fermi level, allowing tunneling between states propagating in opposite directions. Thus, enhanced tunneling is expected between the wires at $B^{i,j}_1$,$B^{i,j}_2$ (Fig. 3B). These crossing points allow an independent measurement of the density of electrons in each mode, the only parameter needed to completely determine the noninteracting dispersion. Determining the density by this method does not depend on the strength of the Coulomb interactions. Their presence merely smears the crossing points in the V_{sd}-B plane but does not shift them to different values of B. In reality, such crossing points can be seen very clearly (Fig. 3, A and C).

In our finite cross-section wires, the analysis is slightly complicated by the small changes of density in each mode induced by changing B—for example, as B is ramped up, the lower modes are populated at the expense of the higher ones. This effect is very small for most of the modes in Fig. 3 but has a noticeable effect on the modes that make up the upper crossing point at $B^{1,1}_2 = 7$ T. The simplest quantitative interpretation of the $G(V_{sd},B)$ scans requires the solution of the single-particle Schrödinger equation for the levels in each of the two wires in the presence of B. From the solution, the noninteracting dispersion of the electrons in each of the wires is obtained and overlaid on the data in Fig. 3, A and C. Below we summarize the main results of a calculation based on the data in Fig. 3, A and C, taken from a $L = 6$ μm junction. Reducing L from 10 to 2 μm merely reduces the magnitude of the tunneling current but does not shift the measured dispersions, confirming the fact that only one junction is effectively biased in the contacting scheme. We find that the following transitions best describe our data (*27*): $|u_1\rangle \leftrightarrow |l_1\rangle$, $|u_3\rangle \leftrightarrow |l_2\rangle$, and $|u_2\rangle \leftrightarrow |l_{3,4,5}\rangle$, where the order in the list is of decreasing $B^{i,j}_2$. We conjecture that $|u_3\rangle$ is the 2DEG that occupies the upper QW, giving a two-dimensional density that is consistent with Shubnikov–de Haas measurements. One can see that the density is determined correctly because the calculated dispersions fit the measured $B^{i,j}_{1,2}$'s. In spite of this, they deviate everywhere else from the measured curves. Similar mismatches between measured and calculated dispersions are always observed, suggesting that the noninteracting behavior does not describe the excitation spectrum.

To quantify the deviations from noninteracting behavior, the data were successfully fitted with a noninteracting model with a renormalized mass $m^* = 0.75$ m (*28*) (see Fig. 3A). The conclusion is that we observe an enhancement of the velocity of the collective excitations, relative to the velocity of the excitations in a noninteracting wire, because $v_p/v_F = m/m^*$. Such an enhancement is brought about by Coulomb interactions and is consistent with Luttinger-liquid behavior (*3*). In the simplest case of weak interwire coupling, Luttinger-liquid theory predicts $v_p = v_F/g$ (*25*), where g is a parameter that characterizes the interactions. This yields $g = 0.75$, a value that agrees with values obtained with a different technique for single CEO wires in GaAs (*12*, *29*). A more elaborate fit to the theory requires the incorporation of finite interwire interactions, as well as intermode coupling (*25*), resulting in having several different values of m^* in our phenomenological model. In contrast to the above behavior of the dispersion peaks, their tails seem to terminate at the noninteracting dispersion curve, marked by the thick dashed lines in Fig. 3A. Such behavior may be expected to result from spin-charge separation (*25*), in which the velocity of the spin degrees of freedom is given by the noninteracting velocity, v_F. Another departure from simple noninteracting behavior is the suppression of $G(V_{sd},B)$ near $V_{sd} = 0$, which can be seen in Fig. 3, A and C, as a B-independent, 150-μV-wide

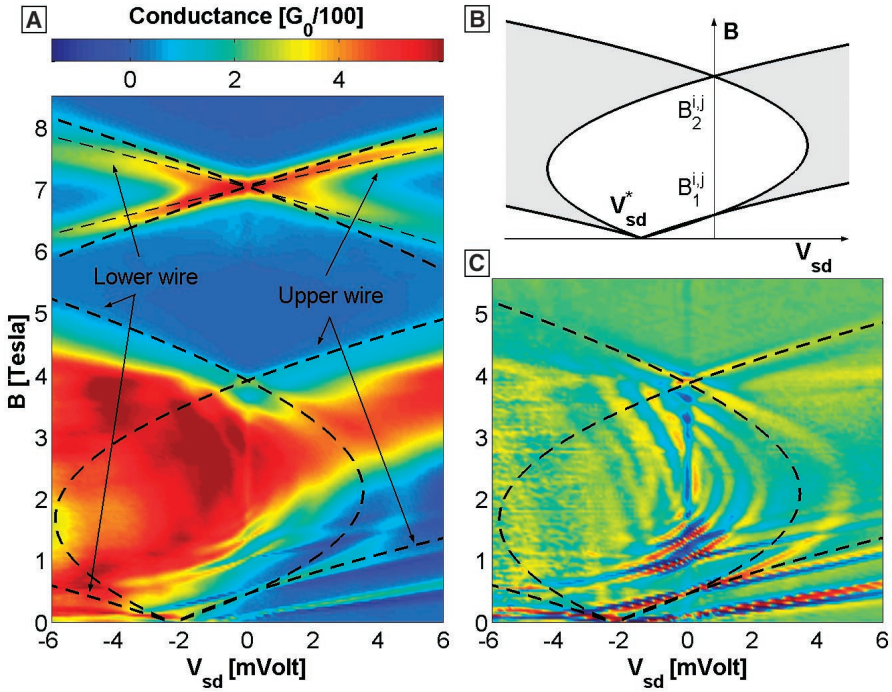

Fig. 3. (**A**) $G(V_{sd},B)$ as a function of V_{sd} and B for a 6-μm-long tunnel junction. The bar above the figure gives the color scale. Some of the dispersions can be easily discerned. The calculated noninteracting dispersions (thick dashed lines) do not describe the data well. A reduced mass model yields a superior fit everywhere, exemplified by the thin dashed lines at high B. The evident enhancement of $G(V_{sd},B)$ at $V_{sd} < 0$ and $B < 5$ T is attributed to tunneling directly from the 2DEG in the upper QW to the LQWR. Also visible is the suppression of $G(V_{sd},B)$ near $V_{sd} = 0$. (**B**) A schematic of the regions of momentum conserving tunneling (gray) for which we expect the tunneling current to be enhanced. At V^*_{sd}, the density mismatch between mode u_i and mode l_j is compensated for and the spectra overlap. Tunneling between the Fermi points of the modes occurs at $B^{i,j}_1$, $B^{i,j}_2$. The boundaries, which show up as peaks in $G(V_{sd},B)$, give the dispersions of the electrons. (**C**) The lower part of (A) after subtracting a smoothed background. The scale has been optimized to improve the visibility. The dispersions of the various bands in both wires are easily discerned, as well as the suppression of $G(V_{sd},B)$ around $V_{sd} = 0$.

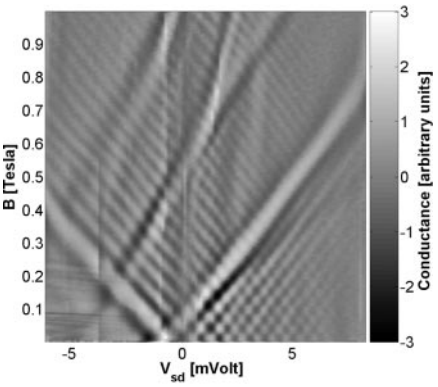

Fig. 4. $G(V_{sd},B)$ for a 2-μm-long tunnel junction at low B. A smoothed background has been subtracted to emphasize sharp features, although these are quite clear in the raw data. Oscillations are seen off the dispersion curves, several of which are easy to see.

dip. These last two effects are of particular interest because both the separation of spin and charge and the suppression of tunneling near $V_{sd} = 0$ are hallmarks of Luttinger-liquid behavior (*3*).

It is interesting to find what limits the conservation of momentum in the experiment and how this shows up in the measurement. Clearly, any mechanism that breaks invariance to translations relaxes the constraint of momentum conservation and with it the conditions for allowing current to flow through the junction. Because of the high quality of CEO wires, momentum relaxation is mainly caused by the finite length of the tunnel junction.

The effects of finite size on $G(V_{sd},B)$ are very clear in the measurement of a 2-μm tunnel junction. Figure 4 shows a zoom into the low B part of such a scan. Even for such a short junction, one can see the dispersions of the wires. On the other hand, contrary to the scan of the 6-μm junction in Fig. 3, $G(V_{sd},B)$ is appreciable off the dispersions. One can see that the deviations of $G(V_{sd},B)$ from zero form a checkerboard pattern. This pattern is a striking manifestation of the finiteness of L: The momentum δ function (that traces out the dispersion curves) oscillates as a function of its argument on a scale L^{-1}; for a 6-μm junction, periods that are one-third of the periods in Fig. 4 are observed. By viewing the checkerboard as Aharonov-Bohm oscillations, it is easy to show that the periods in the V_{sd} and B directions are indeed given by $\Delta V_{sd} L/v_p = \Delta BLd = \phi_0$, where $\phi_0 = h/e$ is the flux quantum. This result can be also derived from a Fermi-liquid microscopic model (*30*). Similar oscillations appear in calculations that take interactions into account (*31*, *32*).

References and Notes

1. P. Nozières, *Theory of Interacting Fermi Systems*, *The Advanced Book Program* (Addison-Wesley, Reading, MA, ed. 2, 1997).
2. B. L. Altshuler, A. G. Aronov, in *Electron-Electron Interaction in Disordered Systems*, A. L. Efros, M. Pollak, Eds. (North-Holland, Amsterdam, 1985), pp. 1–153.
3. V. J. Emery, in *Highly Conducting One-Dimensional Solids*, J. T. Devreese, R. P. Evrard, V. E. van Doren (Plenum, New York, 1979), pp. 247–303.
4. D. Yue, L. I. Glazman, K. A. Matveev, *Phys. Rev. B* **49**, 1966 (1994).
5. Y. Oreg, A. M. Finkel'stein, *Phys. Rev. B* **54**, R14265 (1996).
6. R. de Picciotto, H. L. Stormer, L. N. Pfeiffer, K. W. Baldwin, K. W. West, *Nature* **411**, 51 (2001).
7. D. L. Maslov, M. Stone, *Phys. Rev. B* **52**, 5539 (1995).
8. D. L. Maslov, *Phys. Rev. B* **52**, 14368 (1995).
9. I. Safi, H. J. Schulz, *Phys. Rev. B* **52**, 17040 (1995).
10. V. V. Ponomarenko, *Phys. Rev. B* **52**, 8666 (1995).
11. Y. Imry, *Introduction to Mesoscopic Physics* (Oxford Univ. Press, Oxford, 1997).
12. O. M. Auslaender *et al.*, *Phys. Rev. Lett.* **84**, 1764 (2000).
13. T. Kleimann, M. Sassetti, B. Kramer, A. Yacoby, *Phys. Rev. B* **62**, 8144 (2000).
14. M. Bockrath *et al.*, *Nature* **397**, 598 (1999).
15. H. W. C. Postma, T. Teepen, Z. Yao, M. Grifoni, C. Dekker, *Science* **293**, 76 (2001).
16. R. Goñi *et al.*, *Phys. Rev. Lett.* **67**, 3298 (1991).
17. M. Sassetti, B. Kramer, *Phys. Rev. Lett.* **80**, 1485 (1998).
18. L. N. Pfeiffer *et al.*, *Microelectron. J.* **28**, 817 (1997).
19. G is measured at $T = 0.25$ K with standard lock-in techniques, in which a fixed excitation voltage of 10 μV is applied at a frequency of 14 Hz.
20. A. Yacoby, H. L. Stormer, K. W. Baldwin, L. N. Pfeiffer, K. W. West, *Solid State Commun.* **101**, 77 (1997).
21. R. de Picciotto *et al.*, *Phys. Rev. Lett.* **85**, 1730 (2000).
22. J. P. Eisenstein, L. N. Pfeiffer, K. W. West, *Appl. Phys. Lett.* **58**, 1497 (1991).
23. W. Kang, H. L. Stormer, L. N. Pfeiffer, K. W. Baldwin, K. W. West, *Nature* **403**, 59 (2000).
24. Being coplanar with the 2DEG, the only influence of B on it is by the Zeeman effect. This effect is negligible in GaAs in the B range that we use.
25. D. Carpentier, C. Peça, L. Balents, preprint available at xxx.lanl.gov/abs/cond-mat/0103193.
26. U. Zülicke, M. Governale, preprint available at xxx.lanl.gov/abs/cond-mat/0105066.
27. The densities that we find for the UQWR are $n_{u_i} = 95 \pm 1$, 68 ± 1, and 64.9 ± 0.8 μm^{-1}, and those for the LQWR are $n_{l_j} = 92 \pm 1$, 50.9 ± 0.8, 36.9 ± 0.9, 29 ± 1, and 21.6 ± 0.9 μm^{-1}.
28. The densities with $m^* = 0.75$ m are $n_{u_i} = 99 \pm 1$, 68 ± 1, and 65.6 ± 0.8 μm^{-1} and $n_{l_j} = 95 \pm 1$, 50.9 ± 0.8, 37.2 ± 0.9, 29 ± 1, and 21.0 ± 0.9 μm^{-1}.
29. We attribute the weakness of the interactions to screening by the 2DEG. In fact, the screening length, the width of the wires, and the spacing between them are on the same length scale.
30. O. E. Raichev, P. Vasilopoulos, *J. Phys. Cond. Mat.* **12**, 6859 (2000).
31. M. Sassetti, B. Kramer, personal communication.
32. D. Boese, M. Governale, A. Rosch, U. Zülicke, *Phys. Rev. B* **64**, 085315 (2001).

33. This work is the result of a long-term and fruitful collaboration with H. Stormer. Illuminating discussions with L. Balents, B. Kramer, and M. Sassetti have been very beneficial to us. We also thank B. Halperin, Y. Oreg, A. Stern, and U. Zülicke for helpful conversations. This work is supported by the U.S.-Israel Binational Science Foundation and by a research grant from the Fusfeld Research Fund. O.M.A. is supported by a grant from the Israeli Ministry of Science.

14 September 2001; accepted 19 December 2001

Mapping the One-Dimensional Electronic States of Nanotube Peapod Structures

D. J. Hornbaker,[1] S.-J. Kahng,[1]* S. Misra,[1] B. W. Smith,[2] A. T. Johnson,[3,4] E. J. Mele,[3,4] D. E. Luzzi,[2,4] A. Yazdani[1]†

Arrays of C_{60} molecules nested inside single-walled nanotubes represent a class of nanoscale materials having tunable properties. We report electronic measurements of this system made with a scanning tunneling microscope and demonstrate that the encapsulated C_{60} molecules modify the local electronic structure of the nanotube. Our measurements and calculations also show that a periodic array of C_{60} molecules gives rise to a hybrid electronic band, which derives its character from both the nanotube states and the C_{60} molecular orbitals.

Single-walled carbon nanotubes (SWNTs) have inspired remarkable advances in science and engineering at the nanometer scale during the past decade (*1*). For electronic applications, the SWNT appears to be an ideal template for fabricating single-molecule–based devices, such as nanotube-based diodes (*2–4*), single-electron transistors (*5*, *6*), memory elements (*7*), and logic circuits (*8*, *9*). Due to their size and geometry, SWNTs also provide a unique opportunity for nanoscale engineering of novel one-dimensional (1D) materials systems, created by self-assembly of atoms or molecules inside the SWNT's hollow core (*10*). The promise of this material synthesis method has been demonstrated recently by the discovery (*11*) and subsequent high-yield production (*12*) of C_{60}@SWNT: a supramolecular assembly resembling a nanoscopic peapod composed of a 1D array of C_{60} molecules nested inside a SWNT (Fig. 1A). The composite nature of C_{60}@SWNT peapods, as well as other simi-

[1]Department of Physics and Frederick Seitz Materials Research Laboratory, University of Illinois at Urbana–Champaign, Urbana, IL 61801, USA. [2]Department of Materials Science and Engineering, [3]Department of Physics and Astronomy, [4]Laboratory for Research on the Structure of Matter, University of Pennsylvania, Philadelphia, PA 19104, USA.

*Present address: Department of Physics, Soongsil University, Seoul, Korea.

†To whom correspondence should be addressed. E-mail: ayazdani@uiuc.edu